THE ASTROPHYSICAL JOURNAL, 421:705–717, 1994 February 1

X-RAY EMISSION FROM NEAR–MAIN-SEQUENCE B STARS

J. P. CASSINELLI,[1] D. H. COHEN,[1] J. J. MACFARLANE,[1] W. T. SANDERS,[2] AND B. Y. WELSH[3]

Received 1993 April 5; accepted 1993 July 12

ABSTRACT

Results of a *ROSAT* X-ray survey of 12 nearby near–main-sequence B stars are presented. Objects with very low interstellar hydrogen column density were chosen to study the soft X-ray emission properties of the stars. All of the stars were detected at the 3 σ level. Spectral fits to seven of the stars are presented, and temperatures and source emission measures are derived. The spectra and characterized by emission from gas at a temperature of about 2×10^6 K, which is lower than that typically observed for O stars. The ratio $L_X/L_{\rm Bol}$ decreases sharply with spectral types later than B1, reaching values of about 10^{-9} at B3 V; much less than the value of 10^{-7} that holds for O stars and early-B stars. The survey includes four β Cephei stars and two Be stars. Our observations are consistent with the finding that β Cephei variables have softer spectra than other stars of the same spectral type. The X-ray emission measures for the stars are compared with upper and lower limits derived using mass loss rates and terminal velocities from line-driven wind theory. It is concluded that if shocks embedded in the winds are the source of the X-ray emission then a significant fraction of the winds in B stars must be hot. One to a few shocks can account for the observed emission measures. As a function of spectral type, there appears to be a transition in X-ray emission properties at about B1 to B1.5, with later type stars having a smaller $L_X/L_{\rm Bol}$ ratio. Coronal and shock models are discussed in regards to the B0 V star τ Sco which has an anomalously high source temperature.

Subject headings: shock waves — stars: early-type — stars: mass loss — X-rays: stars

1. INTRODUCTION

Surveys with the *Einstein Observatory* more than a decade ago showed that essentially all O stars and early-B supergiants are X-ray emitters, with luminosities given by the relation $L_X \sim 10^{-7} L_{\rm Bol}$ (Harnden et al. 1979; Long & White 1980; Pallavicini et al. 1981; Cassinelli et al. 1981). The X-ray spectra of the stars indicated emission from a hot gas at temperatures of typically 3 to 9×10^6 K (Chlebowski, Harnden, & Sciortino 1989).

X-ray emission from these stars had been predicted from the appearance of superionization stages such as O VI in the *Copernicus* satellite observations of many early-type stars (Cassinelli & Olson 1979). These initial X-ray emission predictions were based on models in which a hot corona was assumed to exist at the base of the stellar wind. A dynamical coronal model was developed by Waldron (1984). The spectra, however, showed that this could not be the full explanation because there was too little absorption of the coronal emission by the material in the intervening wind (Long & White 1980; Cassinelli et al. 1981). Lucy & White (1980) and Lucy (1982) proposed that the X-rays in O stars arise from shocks that can form because of instabilities in line driven winds. Further studies of the formation of shocks in hot star winds were carried out by Owocki & Rybicki (1984) and Owocki, Castor, & Rybicki (1988).

From an analysis of high-resolution solid state spectrometer (SSS) data for OB supergiants, Cassinelli & Swank (1983) concluded that most of the X-ray emission from OB stars comes from regions well above a base coronal zone, at absorption column densities which correspond to the location where the wind has reached about 90% of its terminal speed. However, there could also be a contribution from much hotter zones, perhaps closer to the star, as evidenced by hard emission components in the SSS spectra and some evidence of a spectral line feature near 2.2 keV in the spectrum of ζ Ori (Cassinelli & Swank 1983).

B stars in luminosity classes III–V, which we refer to as B V stars, were also observed by *Einstein* and have been presented by Long & White (1980), Agrawal et al. (1984), and Grillo et al. (1992). The UV resonance lines which show the presence of winds are narrower in the B V stars. This is an indication of a lower wind terminal speed (Friend & Abbott 1986; Bjorkman 1989). These stars also have significantly lower mass-loss rates, as indicated by the weaker UV resonance lines and the wind densities are estimated to be lower by an order of magnitude or more (Snow 1981). The maximum wind velocity determines the maximum jump in speed across a shock in the wind. If the actual shock velocities are proportional to the terminal wind speeds, then the shock velocities and temperatures should also be lower than is the case for O stars.

The nature of shocks in the B V stars has been considered by Lucy & White (1980) and Lucy (1982) in regard to the B0 V star τ Sco. Because the densities in the B V winds are low relative to those of the more luminous O and OB supergiant stars, the cooling time in the postshock flow is increased. The cooling column density was found to be as large as the entire wind column density so that there could not be a sequence of shocks as proposed in the Lucy (1982) model. The problems of wind shocks in stars with low mass loss rates were addressed by MacFarlane & Cassinelli (1989, hereafter MC). In contrast with the model of Lucy & White (1980), and Lucy (1982), MC found that the shocked region could be relatively thin. MC considered a model in which a fast wind catches up with and shocks an earlier wind. This leads to a "driven-wave" shock structure often discussed in regard to the solar wind

[1] University of Wisconsin-Madison, Astronomy Department, 475 North Charter Street, Madison, WI 53706.
[2] University of Wisconsin-Madison, Physics Department, 1150 University Avenue, Madison, WI 53706.
[3] Center for EUV Astrophysics, 2150 Kittredge Street, University of California-Berkely, Berkeley, CA 94720.

(Hundhausen 1985). A forward-reverse pair of shocks is formed with a high-density contact surface possibly occurring in between. The forward shock occurs where the shock zone catches up with the slow wind, and a reverse shock occurs where the fast wind collides with the shock zone. The net effect is that the region can be narrow and denser than estimated by Lucy & White (1980) and Lucy (1982).

Another mechanism for the production of shocks in the outflow from B stars is associated with the presence of disks around the rapidly rotating Be stars. Bjorkman & Cassinelli (1990, 1993) have developed a "wind-compressed disk" (WCD) model in which the disk is maintained by ram pressure confinement by the stellar wind. Using line-driven wind theory to describe the outflow of the wind that originates at high stellar latitudes, the model predicts that for rotation speeds a certain threshold ($\sim 50\%$ of critical speed), the wind converges toward the equator and passes through an oblique standing shock. This compresses the flow to densities that are two to three orders of magnitude larger than those in the polar regions and produces temperatures between 10^5 and 10^6 K in the postshock region.

In summary, there are several shock models as well as a coronal emission model which can possibly explain the presence of X-rays in the B V stars. The goal of our observations has been to obtain spectra that will help to differentiate among models for B V stars and constrain the number, location, and morphology of the shock regions.

In § 2, the properties of the stars in our survey are described and the analysis methods are described. In § 3 the results of the data analysis are reported, and in § 4 there is a comparison of the results with the model predictions.

2. THE *ROSAT* OBSERVATIONS

2.1. *Survey Stars*

The stars in our survey were chosen to satisfy several criteria: (1) proximity, (2) low interstellar hydrogen column density (typically log $N_H < 20$), and (3) full coverage of the late-O and early-B spectral subtypes within the luminosity classes III–V. The basic parameters of the stars are given in Table 1.

The sample contains several classes of B star. There are four β Cephei variables, (α Vir, ξ^1 CMa, β Cen, and λ Sco), and two Be stars (α Eri and η Cen), as well as five classical B stars. The sample also contains the very late O star, μ Col, O9.5 V. This is a well-studied star and serves as a convenient comparison star to link the B star properties with those of the somewhat better understood O stars (Olson & Castor 1981; Chlebowski & Garmany 1991). Another of the survey stars, τ Sco, is perhaps the best studied of the early-B stars (e.g., Lamers & Rogerson 1978) and has long been used in tests of wind and shock models (Lucy & White 1980; Abbott & Friend 1989; Springmann & Pauldrach 1992). Its X-ray emission was measured using both the IPC and SSS instruments on *Einstein* (Collura et al. 1989; Swank 1985).

TABLE 1

STELLAR PARAMETERS

Object	Spectral Type	Distance[b] (pc)	log N_H[b] (cm^{-2})	V[a]	$v \sin i$[c] (km s^{-1})	L_{bol} (ergs s^{-1})
μ Col	O9.5 V	700	19.85	5.16	140	1.5×10^{38}
τ Sco	B0 V	170	20.43	2.84	20	1.6×10^{38}
θ Car	B0.5 V	207	20.28	2.76	150	1.7×10^{38}
β Cen	B1 III	85	19.63	0.61	110	9.5×10^{37}
ξ^1 CMa	B1 III	460	19.20	4.34	10	1.0×10^{38}
α Vir	B1 IV	86	18.80	0.97	135	7.5×10^{37}
λ Sco	B1 V	110	19.23	1.62	145	3.3×10^{37}
η Cen	B1.5 Ve	93	20.11	2.31	345	1.2×10^{37}
α Pav	B2.5 V	57	<18.30	1.94	20	6.5×10^{36}
α Eri	B3 IVe	28	<18.30	0.48	250	5.3×10^{36}
σ Sgr	B3 IV	55	<18.40	2.09	205	7.4×10^{36}
η UMa	B3 V	42	17.80	1.86	195	5.1×10^{36}

[a] From Hoffleit & Jaschek 1982.
[b] From Welsh, Vallerga, & Vedder 1990, Welsh 1991, and B. Y. Welsh, private communication.
[c] From Uesugi & Fukuda 1982.

2.2. *Binarity of Sample Stars*

Some later type main-sequence stars are known to have X-ray luminosities in excess of 10^{30} ergs s^{-1} due to coronal emission (Pallavicini et al. 1981). So a G-dwarf companion, say, could have stronger X-ray emission than a B3 V star. Evolved companions can also contribute significant quantities of soft X-rays to the combined output of the binary system.

There are indications of binarity for several of the stars in our sample. Unfortunately, in many cases it is impossible to ascertain the nature of the binary companion. For α Vir the companion can be identified as a B3 III star, with a 2 day orbital period (Batten et al. 1987). A visual companion of ξ^1 CMa has a magnitude of +14, compared with the primary's magnitude of +4, at a separation of 0.5 (Proust, Ochsenbein, & Pettersen 1981). θ Car is a spectroscopic binary with a companion of unknown spectral type (de Vaucouleurs 1957). α Pav is a spectroscopic binary with a 12 day period. The spectral type of its companion is unknown (Batten, Fletcher, & MacCarthy 1987). η UMa also has a spectroscopic companion of unknown spectral type (Bahng 1958). λ Sco is thought to have a companion which has recently evolved off the main sequence (Koch 1990). Fortunately, for each of these stars we have one or more apparently single stars in the same spectral class, so the binary stars effects should not prevent us from finding reliable tends in X-ray emission versus spectral type.

2.3. *Data Extraction and Reduction*

All our observations where made with the Position Sensitive Proportional Counter (PSPC) aboard *ROSAT*. This instrument is described in the *ROSAT* Mission Description (NASA Research Announcement 91-OSSA-25, Appendix F, 1991) and in Truemper (1982) and Pfeffermann et al. (1988). It has a 2° field of view and spatial resolution of 25″ at 0.93 keV. The PSPC bandpass is from 0.1 keV to 2.5 keV and the spectral resolution is given by $\Delta E/E = 0.43(E/0.93\ \text{keV})^{-0.5}$. In an attempt to enhance the spectral resolution of soft X-rays for some objects, an observation with the boron filter was used in combination with unfiltered observations. This filter blocks X-rays above the 0.188 keV boron absorption edge and below the carbon edge at 0.284 keV, thereby transmitting X-rays from only the lower half of the carbon band. The use of this filter allowed us to derive tighter constraints on the emission properties of α Vir and β Cen.

The data extraction and spectral analysis were done using the PROS analysis software, which runs within IRAF. The sources were extracted using a circle with a 4′ radius. This is large enough to include any soft photon "electronic ghost images." The background region was extracted from an annulus with an outer radius of $\sim 8'$, or more if the field was not crowded, surrounding the source region. The five objects

TABLE 2

OBSERVATIONAL DATA

Object	Date	Filter	Duration of Exposure (s)	Hardness Ratio[a]	Counts Background Subtracted
μ Col	1992 Mar 31		3962	-0.44 ± 0.05	638 ± 31
τ Sco	1991 Mar 2		931	$+0.61 \pm 0.03$	1413 ± 39
θ Car	1992 Oct 22		1504	-0.26 ± 0.04	562 ± 24
β Cen	1992 Jul 25		676	-0.59 ± 0.04	728 ± 27
	1992 Jul 25		688	-0.62 ± 0.04	736 ± 28
	1992 Jul 26	Boron	596	$+0.19 \pm 0.10$	104 ± 10
	1992 Jul 26		434	-0.62 ± 0.06	441 ± 21
	1992 Jul 26	Boron	730	$+0.07 \pm 0.10$	100 ± 10
ξ^1 CMa	1992 Apr 5		1991	$+0.30 \pm 0.07$	217 ± 16
α Vir	1992 Jan 23		672	-0.88 ± 0.05	737 ± 28
	1992 Jan 23	Boron	3896	-0.61 ± 0.06	477 ± 23
λ Sco	1991 Feb 28		1384	-0.85 ± 0.06	596 ± 27
η Cen	1992 Aug 12		4033	-0.11 ± 0.16	53 ± 9
α Pav	1991 Mar 25		1171	-0.23 ± 0.20	31 ± 6
α Eri	1991 May 9		1582	-0.83 ± 0.21	54 ± 9
σ Sgr	1991 Mar 31		3184	-1.04 ± 0.44	44 ± 13
η UMa	1992 May 26		2616	-0.70 ± 0.54	23 ± 9
	1992 May 29	Boron	4856		17 ± 10

[a] (Counts in channels 51–201) − (counts in 11–41)/(total counts).

with fewer than 100 counts were extracted using smaller source circles, with radii between 1′ and 2′. This was done to minimize the number of background counts inside the source circle and thus minimize the uncertainty in the count rate. For these low count sources, the use of a smaller source extraction circle can be justified because the number of electronic ghost images should be negligible compared to the count rate uncertainty. Table 2 lists the PSPC exposure times and the net background-subtracted counts for the 12 stars in our sample.

2.4. *Timing Analysis*

As can be seen in Table 2, all of our observations are a few kiloseconds in duration. Only two individual observations have more than 4000 s of continuous data. Several of the stars were observed in segments with gaps in between, and this allowed us to search for variability on timescales of several hours or days in these objects.

ROSAT observations are made with the satellite undergoing a 400 s wobble. The wobble mode is used to prevent the PSPC window support wires from obscuring sources in the field of view (Downes et al. 1991). This procedure can introduce a 400 periodicity (and multiples thereof) into the observed data which must be accounted for when performing time variability analysis.

We tested light curves made with several different binnings against the hypothesis of a constant source. Short periodicities were searched for using Fourier analysis and period folding. We attempted to detect long-term variability by fitting a sloping line to the light curve in each case where the hypothesis of a constant source could be rejected at the 90% confidence level. Where we had more than one observation of the same object, separated by a gap, we compared mean count rates among the different segments. We had the capability of detecting fluctuations on the 20%–30% level which have been reported in OB star X-ray emissions (Agrawal et al. 1984; Collura et al. 1989), although confusion with the spacecraft wobble period was a problem.

Given that pulsations of a star could lead to wind variability and perhaps a fast wind–slow wind interaction, we are especially interested in searching for periodicities in the X-ray spectra of the four β Cephei stars. These objects show optical variability in their sample of β Cephei stars using *Einstein* and found only a weak, several hundred second periodicity in one object, β CMa, which is not one of our program stars.

For no star did we find a significant indication of long-term (periods greater than 1 ks) time variability. Although for three objects, ξ^1 CMa, τ Sco, and λ Sco, we detected variability with peak-to-peak amplitude variations of $\sim$20% (with periods of 625, 125, and 400 s, respectively), we must attribute this temporal variability to the spacecraft wobble.

2.5. *Spectral Fits*

The *ROSAT* PSPC records photon events in 242 energy channels in the spectral range 0.1–2.5 keV. In our reduction procedure the data are rebinned into 33 bins. We generally excluded bins with fewer than 10 counts from our spectral fits. We attempted spectral fits so seven stars which had more than 100 net counts. For the five objects which have fewer than 100 net counts, spectral fitting is not justified, and X-ray luminosities were determined using the appropriate conversion factor between count rate and flux, which is in the range $3–7 \times 10^{-12}$ ergs cm^{-2} counts^{-1} depending on the ISM column density and temperature (NASA Research Announcement 91-OSSA-25, Appendix F, 1991).

Our observed pulse height distributions were fitted with thermal continuum plus line emission spectral models (Raymond & Smith 1977; Raymond 1988). The adjustable parameters were temperature, emission measure, and column density (wind and interstellar combined). The column densities were constrained to be at least as large as the published interstellar values (allowing for observational uncertainty). Models were calculated for various combinations of parameters, corrected for interstellar absorption using Morrison & McCammon (1983) opacities, and convolved with the instrument response function. These models were then compared with the observations and the absolute χ^2 minimum determined in parameter space. The best-fit spectral parameters were used, along with the distance to the object, to find the X-ray lumi-

nosity corrected for interstellar absorption. The best-fit spectral parameters for each star are listed in Table 3 and displayed, with confidence regions, in Figures 1*a*–1*g*. We used the updated version of the PSPC instrument response matrix which was incorporated in the 1992 December 15 release of PROS. This was especially critical for analyzing the boron filter observations.

The χ^2 statistic was used to assess the goodness of fit for the spectral models. Good fits generally had reduced χ^2 values below 2. Fits with reduced χ^2 values below 3 were deemed plausible, although not ideal (see Table 3 for reduced χ^2 values). We were able to find model parameters which led to values below 3 for all seven objects. For one object, τ Sco, a two-component model was required in order to achieve a good fit. In order to determine the extent of the confidence regions in parameter space, we calculated a χ^2 grid in three-dimensional (column density–temperature–emission measure) space. The 68%, 90%, and 99% confidence volumes were defined by $\Delta\chi^2$ values based on the number of free parameters in the models (Lampton, Margon, & Bowyer 1976). We display two-dimensional projections in temperature–column density space of these volumes for the single-component fits to observations of six of the stars, with dashed-line contours indicating the emission measure values (Figs. 1*a*–1*f*).

We attempted two-component spectral fits in the cases of the four objects for which the one-component fits had reduced χ^2 values above 2. As mentioned above, the two-component model was necessary to achieve a plausible fit for τ Sco. In the cases of α Vir and β Cen, we had several different observations of each object. For both stars, fitting a two-component model gave an improved fit for some observations but not for others. When the separate observations were fitted simultaneously, the two-component models showed little improvement over the one-component models. The fit to the observation of θ Car was improved by the use of a two-component model, although the best-fit column density for both components in this case was larger than the combined ISM and theoretical wind values. The X-ray luminosity derived from the two component model agrees to within 10% with that derived from the one-component model. Since the one-component model provided a plausible fit we show the fit and the corresponding confidence contours in Figure 1*b*, although we include the best fit parameters for both models in Table 3.

For most stars in the sample, the line of sight ISM column densities are known with a relatively high degree of accuracy. In several cases the most probable hydrogen column density values derived from the spectral fitting procedure were significantly lower than the published ISM values. For these stars we restricted the search of spectral parameter space to column density values at least as large as the published ISM values (allowing for an uncertainty of typically ± 0.15 in the log). We considered that the tendency for low derived column densities could be due to UV photoelectrons possibly causing spurious counts in the PSPC instrument. Although no such phenomenon has been reported, the objects which we observed are very strong UV sources. In order to test this theory we refitted five of the stars. This time we excluded channels 11 through 20. However, this did not cause the derived column density values to become higher; in fact, they tended to be lower, indicating that an excess of low-energy counts was not the cause of the small derived column densities.

For observations with the boron filter we made use of the additional spectral information by simultaneously fitting the filter and nonfilter observations. In these cases the χ^2 confidence grids enclosed less parameter space than those of either the filtered or unfiltered observations alone.

3. RESULTS

3.1. *Individual Objects*

In this subsection we discuss the individual stars and the results of the spectral and timing analysis for each. We make comparisons between our derived X-ray luminosities and those derived from *Einstein* observations (Chlebowski et al. 1989; Grillo et al. 1992). For four objects, τ Sco, λ Sco, β Cen, and θ Car, we found X-ray luminosities which differed by more than a factor of 2 from those found with the *Einstein Observatory*. The *Einstein* count rate to flux conversion was based on a 0.5 keV (5.8×10^6 K) Raymond-Smith model (Grillo et al. 1992), whereas we used different models for each object.

TABLE 3

DERIVED X-RAY PROPERTIES

Object	log N_H (cm^{-2})	Temperature (10^6 K)	log EM (cm^{-3})	L_X (ergs s^{-1})	L_X/L_{Bol}	χ^2_ν	Degrees of Freedom
μ Col	19.7	2.3	54.5	7.6×10^{31}	5.1×10^{-7}	1.9	16
τ Sco (1-comp)	20.3	9.3	54.3	5.8×10^{31}	3.7×10^{-7}	5.2	24
τ Sco (2-comp)	20.9, 21.3	1.3, 8.6	54.9, 54.4	2.7×10^{32}	1.7×10^{-6}	1.4	21
θ Car (1-comp)	20.2	2.1	54.0	2.4×10^{31}	1.3×10^{-7}	2.7	18
θ Car (2-comp)	20.2, 21.0	1.3, 4.0	53.8, 53.6	2.6×10^{31}	1.4×10^{-7}	0.8	15
β Cen	19.5	2.0	53.4	5.7×10^{30}	6.0×10^{-8}	2.7	77
ξ^1 CMa	19.8	3.7	54.0	2.4×10^{31}	2.4×10^{-7}	0.9	12
α Vir	18.5	1.3	53.2	3.6×10^{30}	4.8×10^{-8}	3.0	31
λ Sco	19.0	1.5	53.1	2.7×10^{30}	8.2×10^{-8}	1.0	14
η Cen[a]	...	...	51.8	9.3×10^{28}	7.8×10^{-9}	...	...
α Pav[a]	...	...	51.2	3.9×10^{28}	6.0×10^{-9}	...	...
α Eri[a]	...	...	50.7	1.2×10^{28}	2.3×10^{-9}	...	...
σ Sgr[a]	...	...	50.7	1.8×10^{28}	2.4×10^{-9}	...	...
η UMa[a]	...	...	51.0	6.7×10^{27}	1.3×10^{-9}	...	...

[a] These objects have fewer than 100 counts so their X-ray luminosities were calculated using the count rate to flux conversion factor, assuming a temperature of 2×10^6 K and using the published ISM N_H.

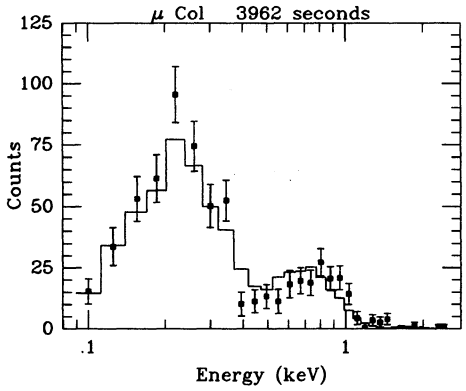

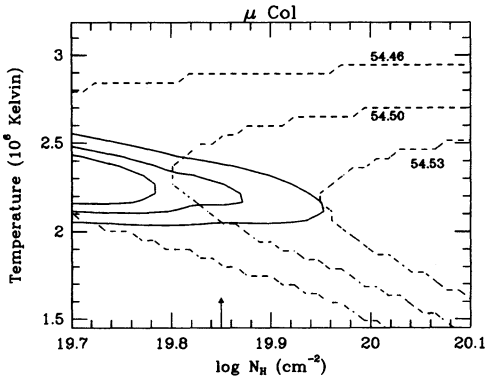

FIG. 1*a*

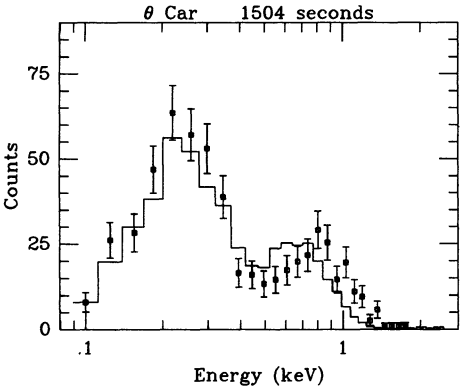

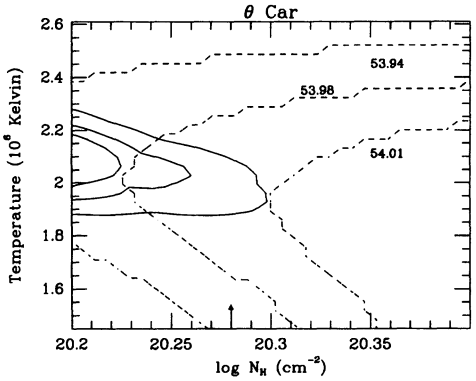

FIG. 1*b*

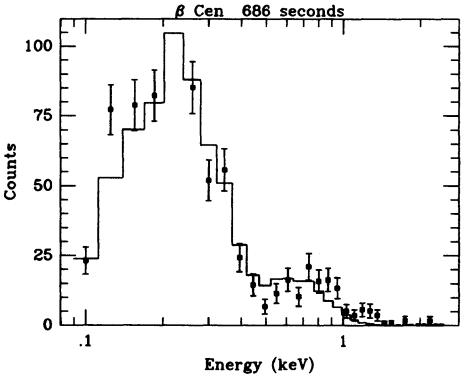

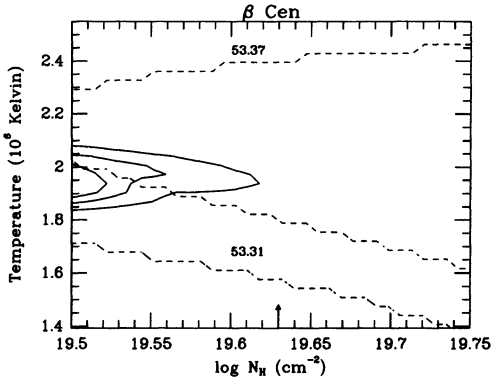

FIG. 1*c*

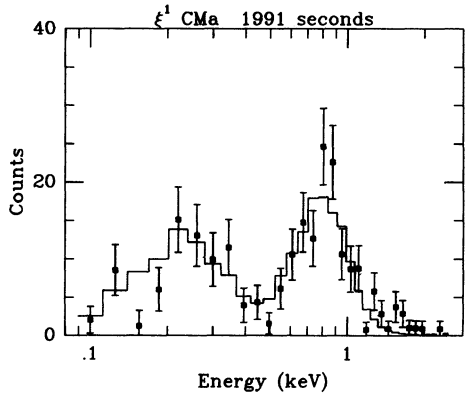

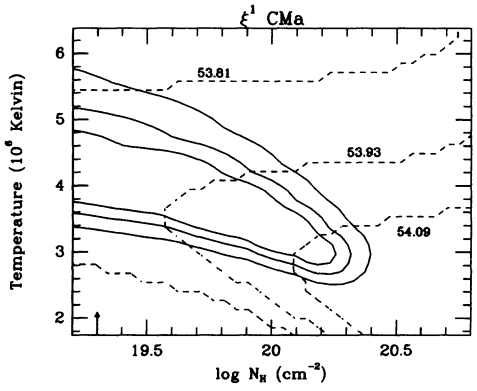

FIG. 1*d*

FIG. 1.—For each pair of figures, the left-hand panel shows the PSPC pulse height distributions in net counts per channel versus energy in keV. Also shown are the best fits to the spectra. The right-hand panel shows the confidence regions in column density–temperature space with the emission measure values indicated with dashed contours. The solid contours show the χ^2 values which correspond to the 68%, 90%, and 99% confidence levels. For τ Sco we show only the pulse height distribution and the one- and two-component models, as the one-component model fit was so poor that the confidence regions are irrelevant and displaying the six-dimensional parameter space of the two-component model fit is problematic.

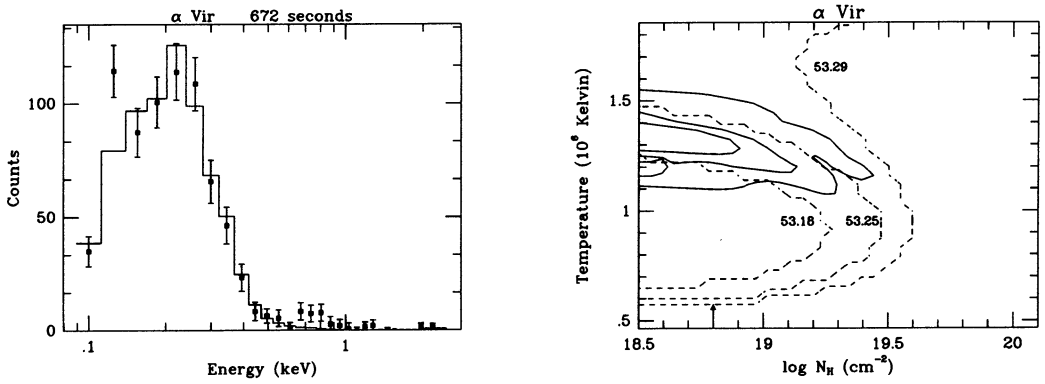

FIG. 1*e*

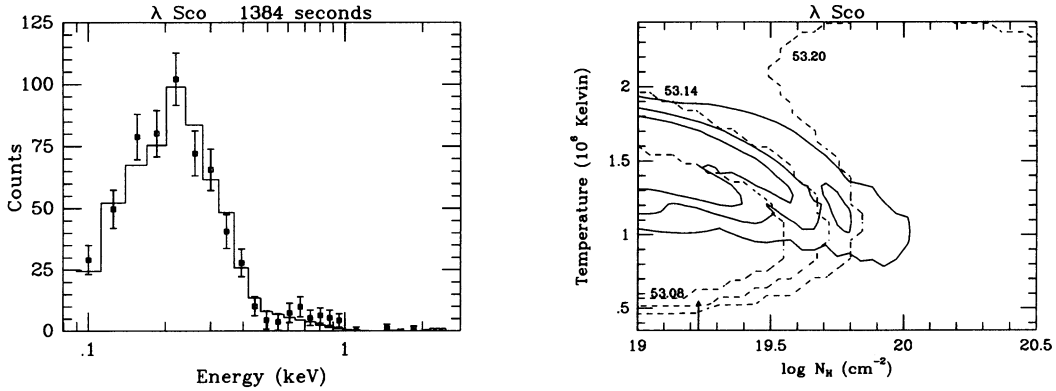

FIG. 1*f*

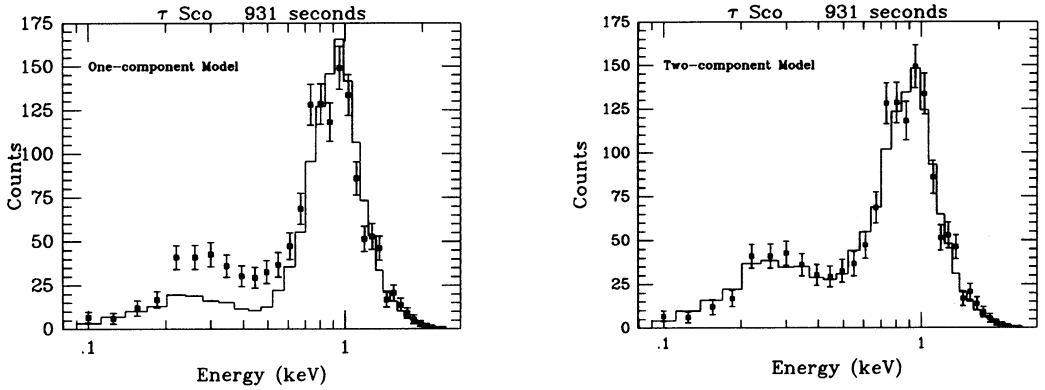

FIG. 1*g*

3.1.1. *μ Col*, O9.5 V

This is the only O star in our sample and serves as a bridge between the early-B stars in our sample and the more thoroughly studied O stars. We therefore note that the X-ray luminosity we found is consistent with that found from *Einstein* IPC observations (Chlebowski et al. 1989). With over 600 counts we had a high-quality observation of μ Col, and therefore the spectral fit was well constrained. The temperature of 2×10^6 K and emission measure of $10^{54.5}$ cm^{-3} were typical for late-O stars, as was the X-ray luminosity of 7.6×10^{31} ergs s^{-1}. There was no evidence of variability in the light curve of μ Col on scales from a few seconds to a few hours.

As we show in § 4.1 the wind is optically thick out to several stellar radii at the lowest energies (see also Table 5), but this did not appear to have an effect on the PSPC spectrum. The derived possible values of the hydrogen column density are in agreement with the ISM value; no additional absorption attributable to the overlying wind was needed. Therefore it appears that the X-rays were emitted from regions farther out in the flow, and certainly not from a base coronal zone. The relatively low temperature of the X-ray–emitting gas is another indication of the absence of a corona.

3.1.2. *τ Sco*, B0 V

τ Sco was our strongest detection with over 1400 counts. The spectral fit indicated that it had the highest temperature of any object in the sample by more than a factor of 2. It also had the highest X-ray luminosity and L_X/L_{Bol} of the stars in the sample.

The single component spectral fit was very poor (see Fig.

1*g*); therefore, we fitted a two-component model to τ Sco, which yielded a significantly better χ^2 value. This model had a component with a temperature around 8×10^6 K and a cooler component with a temperature of about 2×10^6 K. The two components have nearly equal emission measures. The fit indicates that the hot component was seen through a significant amount of absorbing material in the wind. We consider the hot component of the model in more detail in the next section.

Collura et al. (1989) studied *Einstein* IPC observations to search for variability in 12 OB stars. In the case of τ Sco they discovered variability at the 2 σ level with an amplitude of 30% on a time scale of 50 s. We saw no evidence of that periodicity in our observations using either Fourier analysis of the light curve or period folding. Although there was some indication of variability on a timescale of about 125 s, this is probably a harmonic of the spacecraft wobble.

This star was also observed with the *Einstein* SSS (Swank 1985) which revealed the presence of a 5.3×10^6 K and an approximately 20×10^6 K component. We could not detect this hotter component because the emission measure derived by Swank is several times too small for us to have detected in the presence of emission from the other component. The X-ray luminosity we derived (using the two-component spectral fit) of 2.7×10^{32} ergs s^{-1} is several times larger than that found with *Einstein* (Grillo et al. 1992).

3.1.3. θ *Car*, B0.5 V

This star has been reported to be carbon deficient and have enhanced nitrogen, probably due to mass exchange with a binary companion (Walborn 1976). We obtained over 500 counts in our 1500 s observation of θ Car. The temperature we found of 2×10^6 K and the emission measure of about 10^{54} cm^{-3} are very similar to the values we derived for the O star μ Col. The X-ray luminosity we derived of 2.4×10^{31} s^{-1} is more than two times that found with the *Einstein Observatory* for θ Car (Grillo et al. 1992). There was no evidence of any variability for this source on timescales up to several kiloseconds.

3.1.4. β *Cen*, B1 III

This is one of the four β Cephei stars in our sample. We have five separate observations of β Cen each separated by several hours. Two of the observations were with the boron filter and three without. All the spectra had over 100 counts and two have more than 500, although one of the filter observations had only 100 counts and fits to it were not at all well constrained. We therefore fitted models to four of the observations. We found that all four observations could be fitted adequately with a single model. The 90% confidence regions for all four observations overlap in parameter space. By simultaneously fitting the boron and open observations, we took advantage of the added spectral resolution provided by the filter to more tightly constrain the model parameters. This object was found to have a temperature of 2×10^6 K. We derived an X-ray luminosity which is slightly more than twice that found with the *Einstein Observatory* (Grillo et al. 1992). None of the five observations contradicted the hypothesis of a constant source at the 90% level. Additionally, the mean count rate of the three separate unfiltered observations agreed with each other at the 2 σ level. We therefore have no indication of the X-ray emission of β Cen being variable on timescale from 10 to 10^4 s.

3.1.5. ξ^1 *CMa*, B1 III

The β Cephei variable, ξ^1 CMa is the most distant B star in our sample ($D = 460$ pc). Even so, the spectrum was of relatively good quality with over 200 counts recorded. We found a temperature of 3.7×10^6 K, and an emission measure of almost 10^{54}, which is similar to that of τ Sco and μ Col. This star had the strongest X-ray emission of any β Cephei variable in the study of Agrawal et al. (1984). It had the highest L_X of the four β Cephei stars in our sample, with a $L_X/L_{\rm Bol}$ 4 times as large as any of the others. The X-ray luminosity we derived is in agreement with that found with *Einstein* (Grillo et al. 1992). The high luminosity could possibly be due to the presence of a binary companion, at a separation of 0.5. The resolution of the PSPC at the relatively soft energies involved here is too poor to enable us to separate the two sources in the image. If the companion is a flaring M star, it could explain the anomolously hard X-ray spectrum.

Our analysis of the 2000 s light curve of this object indicated the presence of an approximately 650 s periodicity with an amplitude of $\sim$25%. Because this period is near that of the spacecraft wobble, we attribute the variation in the observed intensity to this cause. No variability was detected by Agrawal et al. (1984) using the *Einstein* IPC.

3.1.6. α *Vir*, B1 IV

The β Cephei variable, α Vir (Spica) was observed 4 times, with the observations separated by a total of 3 days. One observation was made without the boron filter and three with it. As with the β Cen observations, we combined the separate data sets for the purpose of spectral fitting. We were able to fit all the observations with a single model and were able to constrain the spectral parameters to a greater degree than we could with any subset of observations. We derived an X-ray luminosity of 3.6×10^{30} ergs s^{-1} which agrees with that found by the *Einstein Observatory* (Grillo et al. 1992) once we account for the different distance (0.04 kpc) used by them. We found no evidence of variability either in the individual observations or from one observation to the next. Thus variability on timescales up to several thousand seconds can be ruled out.

3.1.7. λ *Sco*, B1 V

This was another strong detection with over 500 total counts. We found an X-ray luminosity of 2.7×10^{30} ergs s^{-1} which is almost 3 times larger than that detected by *Einstein*, after allowance for the different distance (0.09 kpc) used by Grillo et al. (1992). λ Sco was one of the softest and weakest sources for which we attempted a spectral fit. There was no evidence of time variability, other than that attributable to the 400 s spacecraft wobble period.

3.1.8. η *Cen*, B1.5 Ve

This object was one of the two Be stars we observed. It has a very low column density and a very rapid rotation speed ($v \sin i = 350$ km s^{-1}). The observation exceeded 4000 s, but we collected only 53 ± 9 counts. This was not enough to justify attempting a spectral fit, but the X-ray luminosity was calculated using a count rate to flux conversion factor of 6.7×10^{-12} ergs cm^{-2} counts^{-1} dictated by the interstellar $N_{\rm H}$ value and assuming a temperature of 2×10^6 K. This calculation gave an X-ray luminosity of 9.3×10^{28} ergs s^{-1}.

3.1.9. α *Pav*, B2.5 V

Our detection of this object (at the 5 σ level with 31 ± 6 counts) was not very strong, and therefore a spectral fit was not

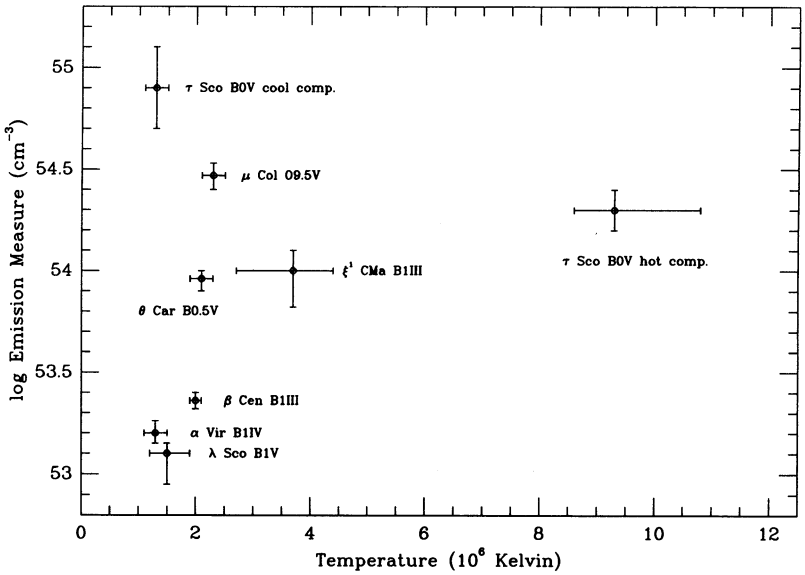

FIG. 2.—Emission measures and temperatures derived from the PSPC observations for seven stars and summarized here. The best-fit values are indicated by the squares, and the error bars correspond to the maximum extent of the 99% confidence contours, calculated with the column densities fixed at the best-fit values. Note that both the hot and cold components are shown for τ Sco.

justified. An X-ray flux was determined using the count rate to flux conversion factor assuming a temperature of 2×10^6 K. Our value of $L_X = 3.9 \times 10^{28}$ ergs s^{-1} is consistent with the upper limit derived from the *Einstein* observation (Grillo et al. 1992).

3.1.10. α *Eri*, B3 IVe

The star α Eri is the nearest Be star ($D = 28$ pc). With 54 ± 9 counts, this was a positive detection, but spectral fitting was not justified. The X-ray luminosity derived from the count rate to flux conversion factor, assuming a source temperature of 2×10^6 K, is 1.2×10^{28} ergs s^{-1}.

3.1.11. σ *Sgr*, B3 IV

This object was a 3 σ detection with 44 ± 13 counts. The X-ray luminosity as derived from the count rate, again assuming a temperature of 2×10^6 K, is 1.8×10^{28} ergs s^{-1}.

3.1.12. η *UMa*, B3 V

We have two observations of this star—one with the boron filter and one without. Neither observation yields a positive detection at the 3 σ level, but taken together, they do constitute a 3 σ detection. However, computing a luminosity from the combined count rate is unreliable. The open observation implies a 3 σ upper limit to the X-ray luminosity of 2.7×10^{28} ergs s^{-1}, assuming a temperature of 2×10^6 K.

For a summary of derived spectral parameters, see Figure 2.

3.2. *The Ratio of X-Ray to Bolometric Luminosity*

Given that the O stars follow the $L_X \sim 10^{-7} L_{Bol}$ relation it is of interest to see if this relation extends to later spectral type. Figure 3 shows our derived values for L_X/L_{Bol} plotted as a function of stellar spectral type. The uncertainties in L_X are due to those of photon counting statistics combined with a factor-of-2 uncertainty in the conversion factor from counts s^{-1} to flux due to uncertainty of the temperature in the X-ray–emitting plasma. We find that the $L_X \sim 10^{-7} L_{Bol}$ relation holds down to spectral type B1, but by B3 the X-ray luminosities are down to a little more than $10^{-9} L_{Bol}$. Only one of our program stars, η Cen, is in the gap between spectral types B1 and B2.5. It is therefore difficult to determine if there is a steady decrease in the L_X/L_{Bol} ratio B1 or if there is an abrupt drop down to the $L_X \sim 10^{-9} L_{Bol}$ regime. An abrupt drop in L_X/L_{Bol} is what would be expected if the line-driving mechanism ceases to function for spectral types beyond the early-B star range (Abbott 1978).

Schmitt et al. (1993) using the HRI on *ROSAT* found that the $L_X \sim 10^{-7} L_{Bol}$ relation extends well down into the B star range for young B stars. Using *ROSAT* all-sky survey data, Meurs et al. (1992) have found that the 10^{-7} law holds for about ~10% of the B stars observed with *ROSAT*. They

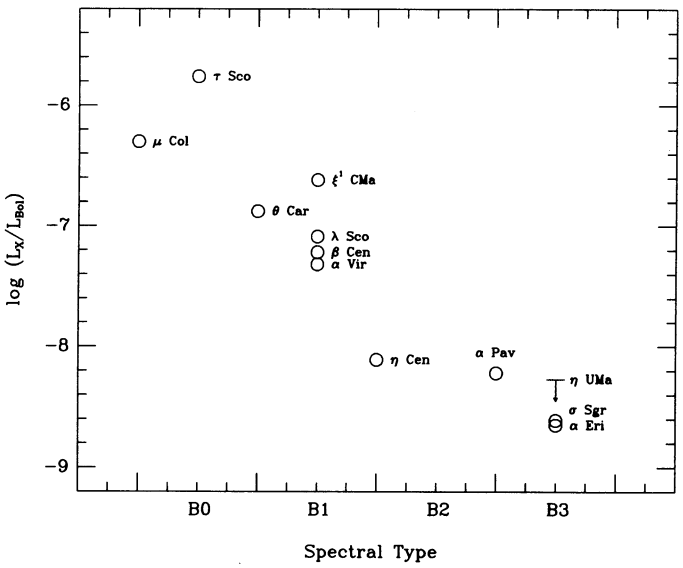

FIG. 3.—The ratio of the X-ray to bolometric luminosity vs. spectral type is shown for all 12 stars. The X-ray luminosities for the seven earliest type stars were calculated from the results of the spectral fitting. The X-ray luminosities for the other five stars were calculated using the appropriate count rate to flux conversion factors. The uncertainties in the L_X/L_{Bol} values are typically a factor of 2, which is on the order of the size of the symbols.

attribute the high L_X/L_{Bol} ratio found for some of the late-B stars in their sample to the presence of binary companions. Our observations appear to describe the variation of L_X/L_{Bol} versus spectral type with less scatter for later spectral types than the results reported by Meurs et al., and our increased sensitivity allows us to detect stars with L_X/L_{Bol} an order of magnitude lower than Meurs et al. (1992). Clearly L_X/L_{Bol} decreases sharply in the B star range.

3.3. *Comments on the β Cephei Stars*

Of the seven objects for which we performed spectral fitting, four were β Cephei variables. The three softest sources are all β Cephei variables: β Cen, α Vir, and λ Sco. The fourth object, ξ^1 CMa, had a relatively hard spectrum with a derived temperature in the 3×10^6 K range, and an X-ray luminosity 6 times greater than any of the other β Cephei variables. This object is known to have a binary companion which could account for the hard radiation. Although our sample is not large enough to allow us to make firm conclusions, the results are consistent with those of Meurs et al. (1992) who found β Cephei variables to have softer X-ray emission than other stars of the same spectral type. There was no more indication of time variability in the X-ray emission of any of the variable stars than there was in the rest of the sample. If the X-ray emission of these stars did vary on the same timescale as the optical emission, then we would have detected it, especially in the cases of α Vir and β Cen, for which which we had several observations spanning many hours, or even days.

4. DISCUSSION

There are several proposed explanations of X-ray production in OB stars. However, we will mostly confine ourselves to interpreting *ROSAT* observations in terms of the presence of shocks in the stellar winds. The star τ Sco has quite different properties from the other stars, and we will discuss the possibility that its hard X-ray spectrum arises from a coronal structure. Although we will be concentrating on thermal emission from shock-heated gas, we will also briefly consider the inverse-Compton emission of shock-accelerated electrons. First, we will discuss radiation-driven wind models, which we use to analyze all the observations.

4.1. *B-Star Properties Based on Wind Models*

In contrast with O stars, very little is known about the winds and mass-loss rates of B stars at spectral type B1 and beyond. The column density through the winds is too small to produce significant wavelength displaced absorption or a P Cygni profile, and so there is little information obtainable from UV line profiles concerning the wind velocities and the wind mass-loss rate for our program stars (except for stars earlier than spectral type B1). Given this lack of information in other spectral bands, and assuming that X-rays arise in wind shocks, X-ray observations therefore can provide useful new information about the winds and outer layers of the atmospheres of B stars. Our approach will be to use theoretical predictions about B star winds and to see if they help us understand the X-ray properties, or if they lead to inconsistencies with the *ROSAT* X-ray emission. We use "modified CAK theory" as described by Friend & Abbott (1986) and Pauldrach, Puls, & Kudritzki (1986). The theory works quite well for the O stars and OB supergiants, and its has led to useful predictions of Be star properties when used in the WCD model (Bjorkman & Cassinelli 1993).

The quantities that determine the wind properties are the stellar parameters: stellar mass, M, luminosity, L, and effective temperature T_{eff}; and the three coefficients of modified CAK theory, k, α, and δ which determine the radiation forces (Abbott 1982). The values of these modeling parameters used for the stars in our survey are presented in Table 4. The values of radiation force parameters were interpolated from the tables in Abbott (1982). Kudritzki et al. (1989) developed a simplified fitting procedure that reproduces quite accurately modified CAK theory results. Their procedure provided the terminal velocity and the mass-loss rates given in Table 4. To calculate wind emission measures we also need to assume a wind velocity law. For this we use the well-known beta velocity law with $\beta = 0.8$ (Groenewegen & Lamers 1989):

$$v(r) = v_\infty(1 - R_*/r)^\beta . \quad (1)$$

For the shocks to provide X-ray emission, there must of course be a jump in velocity that is sufficiently large to produce temperatures of order 10^6 K. Using the relation from Krolik & Raymond (1985),

$$T_X = 1.44 \times 10^5[V_s/(100 \text{ km s}^{-1})]^2 \text{ K} , \quad (2)$$

where V_s is the shock speed relative to the upstream wind velocity, this implies a velocity jump at the shock front of 267 km s^{-1}. This V_s estimate gives some information about the location of the shock; in particular, it can be used to provide a estimate of a minimum preshock wind speed. On inspecting the

TABLE 4

ADOPTED STELLAR PARAMETERS

Object	Spectral Type	T_{eff} (K)	M ($M_\odot$)	log L ($L_\odot$)	V_∞ (km s^{-1})	$\dot{M}$ ($M_\odot$ yr^{-1})	References	k	α	δ
μ Col	O9.5 V	34500	21	4.68	2658	3.22×10^{-8}	1	0.113	0.617	0.121
τ Sco	B0 V	32000	18	4.56	2516	1.63×10^{-8}	1	0.113	0.604	0.095
θ Car	B0.5 V	28000	16	4.54	2038	5.97×10^{-9}	1	0.136	0.577	0.095
β Cen	B1 III	26000	14	4.52	1519	1.88×10^{-8}	1	0.177	0.565	0.116
ξ^1 CMa	B1 III	26000	14	4.52	1518	1.88×10^{-8}	2	0.177	0.565	0.116
α Vir	B1 IV	24000	11	4.30	1280	7.94×10^{-9}	1	0.200	0.552	0.136
λ Sco	B1 V	24000	12	4.26	1385	5.13×10^{-9}	1	0.189	0.554	0.136
η Cen	B1.5 Ve	24000	11	3.98	1585	1.08×10^{-9}	1	0.164	0.556	0.136
α Pav	B2.5 V	17900	7	3.38	1314	5.19×10^{-11}	1	0.161	0.537	0.121
α Eri	B3 IVe	14400	11	3.13	1662	1.42×10^{-11}	3	0.192	0.504	0.041
σ Sgr	B3 IV	18000	7	3.27	1411	2.76×10^{-11}	3	0.152	0.540	0.123
η UMa	B3 V	14400	11	3.13	1474	1.50×10^{-11}	1	0.145	0.541	0.123

REFERENCES.—(1) Snow & Morton 1976; (2) from V magnitude and bolometric correction in Code et al. 1976; (3) Snow 1982.

results of the shock model of Owocki et al. (1988), one sees that the strong reverse shocks tend to have velocity jumps no more than about 0.5 times the local wind speed. Hence if we expect to have shocks of about 267 km s^{-1}, we need to be considering regions where the wind speed is about 500 km s^{-1} or more. We therefore chose to focus our attention on the region beyond the point where the velocity of the wind is equal to some minimum velocity, $v_{\rm min}$. In Table 5 we list the radius at which this minimum velocity is attained.

Now let us consider upper and lower estimates to the emission measure of the X-ray producing material. If a β velocity law structure is assumed, the volume emission measure of the entire wind (beyond the point where the velocity is at least as large as $v_{\rm min}$) is given by

$$\mathrm{EM}_W = (2\beta - 1)^{-1}\ \mathrm{EM}_Z[(v_\infty/v_{\rm min})^{[(2\beta-1)/\beta]} - 1]\ , \quad (3)$$

where EM_Z is the emission measure of a wind having a constant velocity of expansion $v(r) = v_\infty$, is given by

$$\mathrm{EM}_Z = (4\pi/R_*\,\mu_e\,\mu_p)(\dot{M}/4\pi m_{\rm H}\,v_\infty)^2 \quad (4)$$

and μ_e and μ_p are the mean molecular weight per electron and proton, respectively.

An estimate of the minimum X-ray flux associated with stars having numerous source regions in their winds is the emission measure of a single shock. For this, consider a single shock at the base of the X-ray–producing region. We estimate that wind material goes through a reverse shock, heats up to a temperature T_X, and then cools by radiation and adiabatic expansion over a cooling length l_c. The cooling length l_c is related to the characteristic cooling time, t_c, by the relation, $l_c = V_s\,t_c/4$ (Hillier et al. 1993). The characteristic or e-folding cooling time at r is given by

$$t_c = (1.5nkT_X)/(n_e\,n_{\rm H}\,\Lambda + (pv/r)d\ln\rho/d\ln r)\ . \quad (5)$$

Here Λ is the Raymond-Smith emissivity in ergs s^{-1} cm^3, and the last term is the adiabatic cooling rate which we evaluate using the scale length of the local β velocity law at the radius where the shock jump occurs. We find that adiabatic expansion can be the dominant cooling process for stars later than about B1. Cooling times and lengths are given in Table 5.

In addition to the upper and lower limits for the X-ray emission measure, it is useful to know the column density and optical depth through the wind, given by the following integrals over radius or velocity:

$$N_{\rm H} = (\dot{M}/4\pi\mu_{\rm H}\,m_{\rm H})\int_{r_{\rm min}}^{\infty} dr/(vr^2) \quad (6)$$

$$= N_{\rm HZ}/(1-\beta)\ [1 - (v_{\rm min}/v_\infty)^{(1-\beta)/\beta}]\ , \quad (7)$$

where $\mu_{\rm H}$ is the mean molecular weight per hydrogen nucleus, and $N_{\rm HZ}$ is the column density through the wind of a star that has a constant velocity outflow with $v(r) = v_\infty$:

$$N_{\rm HZ} = \dot{M}/(v_\infty\,R_*\,4\pi\mu_{\rm H}\,m_{\rm H})\ . \quad (8)$$

The quantity $N_{\rm HZ}$ is a useful parameter for describing the thickness of a stellar wind. We have found it preferable to plot the X-ray results versus $N_{\rm HZ}$ instead of spectral type. This is because within a given spectral class we can have some stars that are main-sequence stars and some that are giants. On the H-R diagram the two luminosity classes are not widely separated in the B spectral range, but the separation is sufficient to make a noticeable difference in the wind properties. Table 5 includes the $N_{\rm HZ}$ value for each of our stars.

4.2. *Comparison of Observations with B Star Wind Emission Measures*

Figure 4 shows a comparison of the observed EM_X with our upper and lower limits based on wind theory properties, plotted against $N_{\rm HZ}$. Several limits are shown on these figures. We have calculated the upper limit, EM_W using two values for $v_{\rm min}$, 500 km s^{-1} and 267 km s^{-1}, where the latter value is the V_s which produces 10^6 K gas. The lower limit is also calculated in two ways. In one case we use for the shock temperature the value 10^6 K, and in the other case we use the temperature associated with the X-ray spectral fits, to calculate the emission measure in a single spherically symmetric shock zone at the base of the wind with a radial extent equal to the cooling length. Since the T_X associated with the different stars shows a range in values, the line C is rather jagged. Note that for the stars in the spectral class range B0–B1.5 that the observations are nicely bracketed by the upper and lower limits, within the observational and theoretical uncertainties.

For most of the early-B stars, the observed values of the emission measures lie quite close to the EM_1 associated with a single shock. This suggests that number of shocks along any radial column through the star is small. As is discussed in

TABLE 5

STELLAR WIND PARAMETERS

Object	R_{500}[a] (R_*)	log $N_{\rm HZ}$ (cm^{-2})	log $N_{\rm H}(R_{500})$[b] (cm^{-2})	log $N_{\rm H}(2R_*)$ (cm^{-2})	$\tau_{v=500}$ (0.283 keV)	$\tau_{v=500}$ (0.706 keV)	$V_{\rm shock}$[c] (km s^{-1})	$l_c(R_{500})$ (R_*)	$l_c(2R_*)$ (R_*)	$t_c(R_{500})$ (ks)	$t_c(2R_*)$ (ks)
μ Col	1.14	20.93	21.00	20.59	3.28	0.49	400	0.02	0.08	0.77	3.23
τ Sco	1.15	20.65	20.73	20.32	1.69	0.25	770	0.22	0.21	5.06	4.72
θ Car	1.21	20.31	20.34	19.98	0.69	0.10	390	0.11	0.15	4.16	5.40
β Cen	1.33	20.78	20.72	20.45	1.63	0.25	360	0.03	0.08	2.45	5.88
ξ^1 CMa	1.33	20.78	20.72	20.45	1.63	0.25	470	0.09	0.16	4.67	8.29
α Vir	1.45	20.51	20.40	20.18	0.77	0.12	280	0.05	0.09	3.66	6.69
λ Sco	1.39	20.31	20.20	19.98	0.52	0.08	300	0.05	0.09	3.58	6.71
η Cen	1.31	19.72	19.67	19.38	0.15	0.02	267	0.07	0.10	4.16	5.91
α Pav	1.43	18.52	18.41	18.20	0.01	$<10^{-2}$	267	0.15	0.14	7.93	7.62
α Eri	1.29	17.79	17.76	17.46	$<10^{-2}$	$<10^{-2}$	267	0.14	0.12	8.60	7.06
σ Sgr	1.38	18.28	18.20	17.94	0.01	$<10^{-2}$	267	0.15	0.13	6.79	6.23
η CMa	1.35	17.79	17.99	17.72	$<10^{-2}$	$<10^{-2}$	267	0.15	0.13	5.80	5.15

[a] Radius at which $v_{\rm wind} = 500$ km s^{-1}.
[b] Column density above R_{500} (to infinity); $N_{\rm H}(2R_*)$ column density above $2R_*$.
[c] For those stars with fewer than 100 counts, a shock temperature of 10^6 K is assumed.

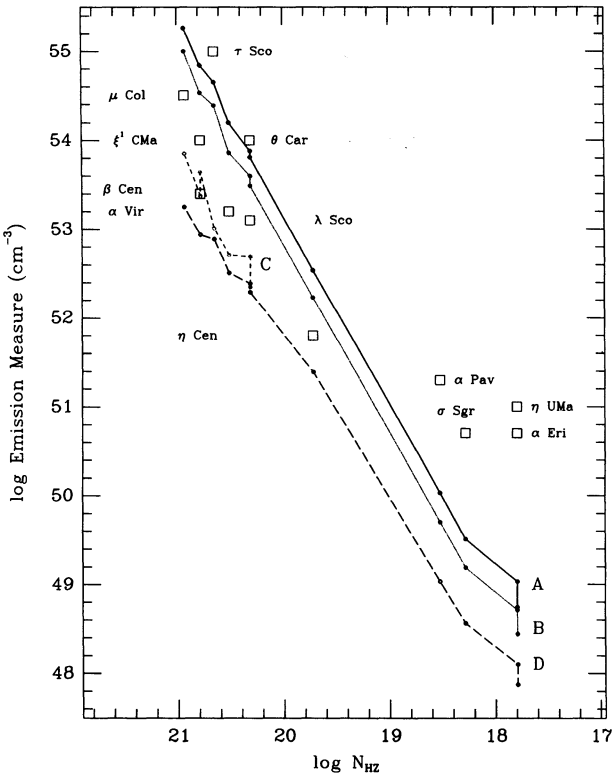

FIG. 4.—Emission measure vs. the column density parameter N_{HZ} (defined in eq. [8]) are shown for each star. The points for each star are taken from the best-fit single-component models or the count rate to flux conversion factors, except in the case of τ Sco, where the value comes from the two-component spectral fit. The four lines shown were derived from standard radiation-driven wind theory, as described in the text. The upper limits (denoted A and B) are integrals over the entire smooth wind from some inner point (v = 267 and 500 km s^{-1}, respectively) out to infinity. The lower limits (C and D) are the expected emission measures from a single shock at the base of the wind. Line C is calculated using the derived emission temperatures, while line D is calculated assuming a temperature of 10^6 K.

Cassinelli & Swank (1983), a smaller number of shocks could lead to significant variability in the X-ray emission as the shocks propagate outward and their X-ray emission decreases. This is certainly the case if the shocks are spherically symmetric about the star. However, if a typical shock subtends a small solid angle above the star, then the X-ray time variability would be relatively constant because the emission arises from a large number of shock zone segments. The lack of demonstrable variability in our sample suggests that the segmented emission picture applies. This was also the conclusion of Cassinelli & Swank (1983) in regards to the OB supergiant stars.

Figure 4 shows a rather different result for the B stars of spectral type B2.5 and B3 (which cluster to the lower right side of the figure). The X-ray emission measure has decreased significantly for these later type B V stars, but not as much as wind theory predicts. The observed emission measures are an order of magnitude above the upper limits. Several explanations are possible:

1. The values used for the ratio $(\dot{M}/v_\infty)^2$ that appears in the expression for the wind emission measure could have been underestimated by our application of line-driven wind theory to B stars later than B2. It is quite possible that the terminal velocity is overestimated. Two recent papers have investigated why B stars do not show broad wind profiles. Abbott & Friend (1989) suggested that the wind is terminated by the fact that the outermost shocks do not cool off and this leads to an upper limit on the velocity since the driving ions are no longer present. Springman & Pauldrach (1992) have argued that the acceleration of a line-driven wind terminates at a radius at which there can be a decoupling of the driving ions and the wind plasma. Either of these explanations could perhaps decrease the terminal speed by a factor of 2 or so. In both of these models it is assumed that the mass-loss rate which is determined by conditions at the flow critical point is not changed. But it is not implausible that the one order of magnitude excess of X-ray emission measure shown in on the right-hand side of Figure 4 could be explained by modifications to the winds that would change $\dot{M}/v_\infty$ by a factor of 3.

2. A second possible reason for an excess emission measure could be that the material is located in a corona. Some support for this possibility is given by the 30 ks *ROSAT* observation of the Be star λ Eri, which shows that it has a flaring hard component attributed to a magnetized region (Smith et al. 1993).

3. The Be stars are rapid rotators and their winds are not spherically symmetric In particular, for the WCD model the winds from the polar regions collide at the equatorial zone and hot gas is produced behind the oblique shock. The shock structure is not like the spherical one that we have envisioned in deriving our estimates of the two limits EM_W and EM_1. The WCD model predicts a higher emission measure than would be expected from our spherically symmetric shock picture, which is exactly what we see in the case of α Eri. The only other Be star in our sample is η Cen, and in Figure 4 it is nevertheless bracketed by the upper and lower limits.

4. The excess emission derived in the cases of α Pav and η UMa could be due to the presence of binary companions around these objects. Such companions could have X-ray luminosities on the order of the observed 10^{29} ergs s^{-1}.

We favor the first explanation, that our application of wind theory has underestimated the $\dot{M}/v_\infty$ for the winds of B stars beyond spectral type B2. The explanation which relies on the presence of coronae seems unlikely because the emission from theses stars is so soft. All of the later type stars in the sample have hardness ratios comparable to or softer than that of θ Car. This implies that none of these objects has a temperature much above 2×10^6 K. The third explanation necessarily applies only to Be stars and therefore cannot be a complete explanation. Likewise, the last explanation can only account for the relatively high X-ray luminosities of two of the four stars.

If we are going to attribute the X-ray production in the objects we have observed to wind shocks, we would like to be able to place the locations of these shocks zones in the winds. As was mentioned in the subsections on the individual stars, the column densities we find from the spectral fitting procedure are generally consistent with no wind absorption. In fact, only for τ Sco, ξ^1 CMa, and θ Car (two-component model) do the spectral fits to the observations allow the possibility of X-rays arising closer to the star than one stellar radius from the surface.

4.3. *Inverse-Compton X-Ray Emission*

Chen & White (1991) have studied in detail a mechanism in which electrons are accelerated to relativistic velocities via multiple passages through wind shock fronts. These relativistic electrons inverse-Compton–scatter UV photospheric photons

up to X-ray energies. This mechanism has been invoked to explain the hard X-ray emission seen from O stars, but its application to B stars is uncertain because the shock structure in B star winds is not well known (Chen 1992). We fitted power-law spectra, as would be expected from this inverse-Compton mechanism, to several of our observations. In the case of τ Sco we obtained a fit for a combined Raymond-Smith and power-law model which was statistically as good as that for a two-component Raymond-Smith model. The power-law index we derived was 2.5. Such a steep spectrum could be produced by electrons which have been accelerated through relatively weak shocks with Mach numbers around two (Chen 1992). In our fit, the power-law component was responsible for producing a few times 10^{32} ergs s^{-1}. While the inverse-Compton luminosity we derive is high, and the spectrum is quite steep, the parameters are possibly consistent with the Chen & White model. Although we cannot rule out the possibility that this shock-related mechanism produces some soft X-rays in some of the objects in our sample, we choose to discuss it no further because of the uncertainty in its application to B star winds.

4.4. *Coronal X-Rays*

It can be seen from the pulse height distribution that τ Sco is an anomolously hard source. Indeed the SSS observations by Swank (1985) revealed an even hotter component. One can ask whether coronal emission could explain our observation. Our two-component fit to the PSPC data indicates that there is a 8×10^6 K component seen through a column density of about 10^{21} cm^{-2}. This column density is consistent with that of the entire wind of τ Sco in addition to the ISM contribution, indicating that the emitting region lies at the base of the wind. The V_s associated with a temperature of 8×10^6 K is about 800 km s^{-1} and so a shock of this magnitude would not form inside the point in the wind where the velocity reaches about 1500 km s^{-1}. But even if the entire wind beyond this point is heated to 8×10^6 K, the emission measure in this region is too small by an order of magnitude to account for the observed emission measure.

This appears to be good evidence for the presence of a coronal zone on τ Sco. However, it was just this sort of problem that was addressed using an alternative shock model by MacFarlane & Cassinelli (1989). A discussed earlier, their model, in which a fast wind collided with a preexisting slower wind, can explain how a large X-ray emission measure could be produced because of the relatively large cooling length of the shock zone. Whether that particular shock model is the best one of τ Sco or whether a coronal contribution is required for the star is still unclear. However, it is clear that none of the other stars in the sample have the high temperatures indicative of coronal emission.

5. CONCLUSIONS

We have obtained X-ray observations for nearby B stars that lie in the spectral range O9.5–B3. For many of the stars the inferred temperature of the X-ray source regions is low relative to that of O stars, which indicates that it would be difficult to detect the stars located at column densities much above 10^{20} cm^{-2}. In the future, the softness of the emission must be accounted for when interpreting statistics based on large samples of B stars.

The L_X/L_{bol} relation that holds for the O stars does not hold for all of the B stars. The ratio decreases from about 10^{-7} to about 10^{-9} along the spectral sequence from B0 to B3. There is a clear difference between the early B V stars and the ones in the mid–B V spectral range. Limits on X-ray emission measures derived from wind theory also show a strong decrease over this spectral range. This change in L_X/L_{Bol} is consistent with the decrease in the amount of wind material present.

Making comparisons with wind theory predictions, we found it convenient to use a measure of the wind column density proportional to $\dot{M}/R_* v_\infty$ instead of spectral class because our sample consists of stars of luminosity classes V, IV, and III, so the wind properties are not monotonic in spectral class alone. The emission measures associated with the observations have been found to be consistent with predictions made on the basis of line-driven wind theory for all of our stars, independent of luminosity class, for spectral classes B0–B1.5. The comparisons are consistent with the picture that X-rays are produced by just a few shock zones because of the relatively large predicted cooling lengths. The lack of time variability in any of the observed objects suggests that the shock-emitting regions are segmented, as opposed to spherically symmetric.

Stars of spectral type B2.5–B3 with small wind column densities have X-ray emission measures that are larger than our estimates for the entire wind emission measure, and four possible explanations have been offered. Perhaps our use of line-driven wind theory that provides reasonable estimates for the B0–B1.5 stars becomes less accurate for later type stars, in the sense that the later type stars have a larger $\dot{M}/v_\infty$ than predicted. Nevertheless the fact that wind theory provides predictions that are reasonably good, gives additional justification for the application of the theory to B stars, as in the WCD models.

We find temperatures for the B V star X-ray–emitting regions of $1–4 \times 10^6$ K (except for τ Sco). This range is about a factor of 2 below the temperatures found for O stars. This is just what is expected in the shock picture if the B V stars have lower terminal velocities than the O stars. Three of the four β Cephei variables have derived temperatures consistent with 1×10^6 K.

The O9.5 star μ Col has X-ray properties similar to the majority of the B stars in the sample. The emission is too cool and too free of absorption to arise in a coronal region.

The star τ Sco appears to be quite different from the other stars in our sample, in that the emission temperature is significantly higher. This might result from a coronal loop source region, analogous to that in λ Eri (Smith et al. 1993). However, it is also possible to explain the results with a fast wind/slow wind interaction shock.

We thank John Finley for his valuable advice regarding *ROSAT* timing and spectral analysis. We are also grateful for useful discussions with Jon Bjorkman, Glenn Cooper, Derck Massa, Geraldine Peters, and Wayne Waldron. This research was supported by NASA grant NAG 5-1579 and NAGW-2210.

REFERENCES

Abbott, D. C. 1978, in IAU Symp. 83, Mass Loss and Evolution of O-Type Stars, ed. P. S. Conti & C. W. H. deLoore (Dordrecht: Reidel), 237
———. 1982, ApJ, 259, 282
Abbott, M. J., & Friend, D. B. 1989, ApJ, 345, 505
Agrawal, P. C., Singh, K. P., Riegler, G. R., & Stern, R. A. 1984, MNRAS, 208, 845
Bahng, J. D. R. 1958, ApJ, 128, 572
Batten, A. H., Fletcher, J. M., & MacCarthy, D. G. 1987, Pub. Dom. Astrophys. Obs. Victoria, 17
Bjorkman, K. S. 1989, Ph.D. thesis, Univ. of Colorado
Bjorkman, J. E., & Cassinelli, J. P. 1990, in Angular Momentum and Mass Loss for Hot Stars, ed. L. A. Willson & G. H. Bowen (Dordrecht: Kluwer), 185
———. 1993, ApJ, 409, 429
Cassinelli, J. P., & Olson, G. L. 1979, ApJ, 229, 304
Cassinelli, J. P., & Swank, J. H. 1983, ApJ, 271, 681
Cassinelli, J. P., Waldron, W. L., Sanders, W. T., Harnden, F. R., Rosner, R., & Vaiana, G. S. 1981, ApJ, 250, 677
Chen, W. 1992, Ph.D. thesis, Johns Hopkins Univ.
Chen, W., & White, R. L. 1991, ApJ, 366, 512
Chlebowski, T., & Garmany, C. D. 1991, ApJ, 368, 241
Chlebowski, T., Harnden, F., & Sciortino, S. 1989, ApJ, 341, 427
Code, A. D., Davis, J., Bless, R. C., & Hanbury Brown, R. 1976, ApJ, 203, 417
Collura, A., Sciortino, S., Serio, S., Vaiana, G. S., Harnden, F. R., & Rosner, R. 1989, ApJ, 338, 296
de Vaucouleurs, A. 1957, MNRAS, 117, 449
Downes, R., White R. E., Reichert, G., Pennerl, K., Englhauser, J., Rosso, C., & Voges, W. 1991, The *ROSAT* Data Products Guide (GSFC: NASA)
Friend, D. B., & Abbott, D. C. 1986, ApJ, 311, 701 (FA)
Grillo, F., Sciortino, S., Micela, G., Vaiana, G. S., & Harnden, F. R., Jr. 1992, ApJS, 81, 795
Groenewegen, M. A. T., & Lamers, H. J. G. L. M. 1989, A&A, 79, 359
Harnden, F. R., Jr., et al. 1979, ApJ, 234, L51
Hillier, D. J., Kudritzki, R. P., Pauldrach, A. W., Puls, J., Baade, D., & Schmitt, J. H. 1993, A&A, in press
Hundhausen, A. J. 1985, in Collisionless Shocks in the Heliosphere: A Tutorial Review, ed. R. G. Stone, & B. T. Tsurutani (Washington: AGU), 37
Hoffleit, D. & Jaschek, C. 1982, The Bright Star Catalogue (New Haven: Yale Univ. Press)
Koch, R. H. 1990, Bull. Inf. CDS, 38, 175
Kudritzki, R. P. Pauldrach, A., Puls, J., & Abbott, D. C. 1989, A&A, 219, 205
Krolik, J. H., & Raymond, J. C. 1985, ApJ, 298, 660
Lampton, M., Margon, B., & Bowyer, S. 1976, ApJ, 208, 177
Lamers, H. J. G. L. M., & Rogerson, J. B. 1978, A&A, 66, 417
Long, K. S., & White, R. L. 1980, ApJ, 239, L65
Lucy, L. B. 1982, ApJ, 255, 286
Lucy, L. B., & White, R. L. 1980, ApJ, 241, 300
MacFarlane, J. J., & Cassinelli, J. P. 1989, ApJ, 347, 1090 (MC)
Meurs, E. J. A., et al. 1992, A&A, 265, L41
Morrison, R., & McCammon, D. 1983, ApJ, 270, 119
Olson, G. L., & Castor, J. I. 1981, ApJ, 244, 179
Owocki, S. P., Castor, J. I., & Rybicki, G. B. 1988, ApJ, 335, 914
Owocki, S. P., & Rybicki, G. B. 1984, ApJ, 284, 337
Pallavicini, R., Golub, L., Rosner, R., Vaiana, G. S., Ayres, T., & Linsky, J. L. 1981, ApJ, 248, 279
Pauldrach, A. W. A., Puls, J., & Kudritzki, R. P. 1986, A&A, 164, 86
Pfeffermann, E., et al. 1988, Proc. SPIE, 733, 519
Proust, D., Ochsenbein, F., & Pettersen, B. R. 1981, A&AS, 44, 179
Raymond, J. C. 1988, in Hot Thin Plasmas in Astrophysics, ed. R. Pallavicini, (Dordrecht: Kluwer), 3
Raymond, J. C., & Smith, B. W. 1977, ApJS, 35, 419
Schmitt, J. H. M. M., Zinnecker, H., Cruddace, R., & Harnden, F. R. 1993, ApJ, 402, L13
Smith, M. A., Grady, C. A., Peters, G. J., & Feigelson, E. D. 1993, ApJ, 409, L49
Snow, T. P. 1981, ApJ, 251, 139
———. 1982, ApJ, 253, L39
Springman, U., & Pauldrach, A. W. A. 1992, A&A, 262, 515
Swank, J. H. 1985, in The Origin of Nonradiative Heating/Momentum in Hot Stars, ed. A. B. Underhill & A. G. Michalitsianos (NASA Conf. Publ. 2358), 86
Truemper, J. 1982, Adv. Space Res., 2, 241
Uesugi, A., & Fukuda, I. 1981, Revised Catalogue of Stellar Rotation Velocities (Kyoto: Kyoto Univ.)
Walborn, N. R. 1976, ApJ, 205, 419
Waldron, W. L. 1984, ApJ, 282, 256
Welsh, B. Y. 1991, ApJ, 373, 556
Welsh, B. Y., Vallerga, J. V., & Vedder, P. W. 1990, ApJ, 358, 473
Welsh, B. Y., Vedder, P. W., Vallerga, J. V., & Craig, N. 1991, ApJ, 381, 462